Simple model for pyroelectric luminescence

J. Kalinowski and Z. Dreger
Department of Molecular Physics, Technical University of Gdańsk, PL-80-952 Gdańsk, Poland
(Received 25 March 1987)

A typical mode of pyroelectric luminescence (PEL) consists of repeated bursts of light, with the intensity and repetition rate of the light pulses dependent on properties of the crystal, rate of its temperature change, and characteristics of the ambient atmosphere. We treat this luminescence pattern by employing the balance equation of charge at the crystal surface. We include generation of the surface charge by temperature change of the spontaneous polarization and the compensation of this charge by intrinsic as well as extrinsic electrical conductivity of the crystal. Good agreement is obtained between the model and the measured PEL of an *N*-isopropylcarbazole single crystal.

I. INTRODUCTION

Pyroelectric crystals subject to changing temperature emit light which is called pyroelectric luminescence (PEL).[1-8] The nature of PEL is different from that of thermoluminescence (TL). While TL should be strictly reserved for light emission produced by heating of previously irradiated samples, PEL is spontaneous light emission occurring without earlier irradiation on their heating and on their cooling as well. Hanson *et al.*[1,3,5] distinguish different types of PEL based on the dependence of the emission features on the pressure of the ambient gas. In class I, under pressure ranging from 10^5 to 10^2 Pa, the luminescence consists of periodic bursts of light. Class-II luminescence, appearing in the pressure range 10^2-10^{-1} Pa, consists of bursts of light preceded by a series of less-intense pulses. Finally, in class III, under pressures below 10^{-1} Pa, the luminescence varies gradually with temperature, usually over a relatively narrow temperature range, and peaks at a temperature characteristic of the crystal. Class-I PEL is thought to originate from electric breakdown in the ambient atmosphere.[1-8] The luminescence in class II seems to have the same origin—the less-intense pulses being small discharges over shorter distances on the crystal surface.[1,3,5,7] The luminescence under class-III conditions is radically different from classes I and II and is suggested to originate from charge carrier recombination,[1,3,5] though similar luminescence effects have also been observed at structural phase transitions induced by temperature[4,7] and pressure[9] variations. A strong luminescence upon heating has been reported for some ferroelectric crystals at the Curie temperature.[6,10,11]

We shall concentrate on the PEL of class I which most directly represents pyroelectric properties of crystals. This genuine pyroelectric luminescence is a result of the temperature-induced change in the spontaneous polarization, accompanied by the electric field growing along the pyroelectric axis of the crystal. When the resulting increase in field strength becomes sufficiently high, the electric breakdown of the ambient gas takes place—a light signal appears to be recorded by the optical detection system. Further, since the polarization in the pyroelectric crystal is compensated by free charges acquired from the surrounding medium, the breakdown ceases and the light signal disappears. The continuous temperature change will start to build up the field up to the next breakdown. In this way the light detected takes on the form of repeated bursts, their repetition time dependent on geometry and physical properties of the crystal, rate of the temperature change, and characteristics of the ambient atmosphere.

A quantitative analytical investigation of the influence of all these factors on the repetition time appears to us to be extremely difficult (if possible), and has not been attempted. Instead, we have investigated this problem using a phenomenological approach to processes underlying PEL.

In this paper we outline a simple phenomenological model for PEL and report on results of temperature and gas-pressure dependences of the repetition rate of light pulses. The effects of the temperature rate of change and the secondary ionization coefficient of the gas are shown. Finally, the results obtained from the model are compared with experimental results for an *N*-isopropylcarbazole single crystal.

II. THE MODEL

Let us consider an ideal pyroelectric single crystal placed in a continuous gas medium of dielectric permittivity ϵ_g. Suppose that the crystal is a parallelepiped with its pyroelectric axis directed along coordinate axis z (Fig. 1). The spontaneous polarization (P) and dielectric permittivity (ϵ) of the crystal determine the spontaneous polarization field (see, e.g., Ref. 12)

$$E_S = P/\epsilon_0\epsilon = (\epsilon_0\epsilon V)^{-1}\int_V \mu_i dV \ , \tag{1}$$

where ϵ_0 is the dielectric permittivity of free space. In (1) P is expressed by the microscopic dipole moment μ_i of the crystal with the integral running over its total volume V.

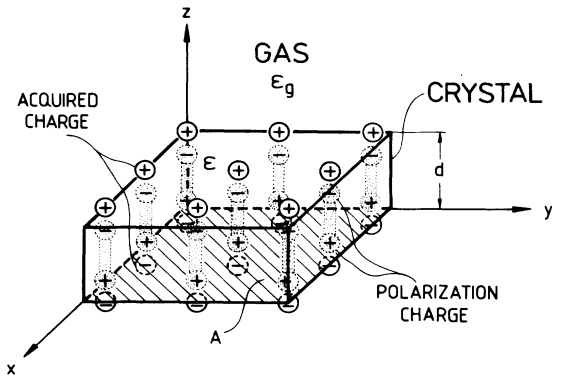

FIG. 1. Three-dimensional representation of a pyroelectric crystal under steady-state conditions with ambient atmosphere.

The field in the crystal near-edge region of the gas corresponds to E_S through the simple relation

$$E_g=\frac{\epsilon}{\epsilon_g}E_S \ . \tag{2}$$

At gas pressures $p \lesssim 10^5$ Pa, ϵ_g is usually smaller than ϵ, so that E_g exceeds E_S, making the probability of the electrical breakdown of the gas greater than that of the crystal itself.

Changes in polarization field can be deduced from the changes in the charges on the planes perpendicular to the pyroelectric axis (planes $z=0$ and $z=d$ in Fig. 1). Hence

$$E_g=\frac{\sigma_S}{\epsilon_0\epsilon_g} \ , \tag{3}$$

where σ_S is the surface density of charge (a charge per unit area).

If the crystal is uniformly heated (cooled) then E_S appearing in the crystal is a measure of its pyroelectricity and the pyroelectric coefficient defined by

$$p(T)=\epsilon_0\epsilon\frac{dE_S}{dT} \ . \tag{4}$$

The changing temperature of the crystal can thus be treated as the generator of net charge $\Delta\sigma_S$ on its external z planes and the crystal itself as a parallel-plate capacitor with two electrodes of area A with equal but opposite charges. On the other hand, due to the finite conductivity of the crystal, the "capacitor plates" will be continuously discharged.

The field E in the crystal may reach the value of the breakdown field strength E_b only if the charge generation rate exceeds the rate of its compensation. In this case, the balance equation may be written as

$$\epsilon_0\epsilon(T)\frac{dE(T)}{dt}=p(T)\frac{dT}{dt}-\sigma(T)E(T) \tag{5}$$

or

$$\epsilon_0\epsilon_g(T)\epsilon(T)\frac{dE_g}{dt}=\epsilon(T)p(T)\frac{dT}{dt}-\epsilon_g(T)\sigma(T)E_g(t) \ . \tag{6}$$

The proportionality factor in the second term of the right-hand side of (5) [$\sigma(T)$] is the temperature-dependent effective electrical conductivity of the crystal. $\sigma(T)$ consists essentially of two components, one due to the bulk conductivity of the crystal in the direction of the pyroelectric axis and the other for which the charge moves on the surfaces having nonzero projections onto the planes parallel to this axis.

A uniform rate (β) of temperature change is normally used so that

$$T=T_0+\beta t \ , \tag{7}$$

where T_0 is the temperature at time $t=0$, $\beta>0$ for heating, and $\beta<0$ for cooling.

Carrying out the integration in Eq. (6), the resulting expression for the near-crystal-edge field is then given by

$$E_g(T)=W^{-1}(T)\left[E_g(T_0)+\epsilon_0^{-1}\int_{T_0}^{T}\epsilon_g^{-1}(T')p(T')\times W(T')dT'\right] \ , \tag{8}$$

where

$$W(T)=\exp\left[(\beta\epsilon_0)^{-1}\int_{T_0}^{T}\epsilon^{-1}(T')\sigma(T')dT'\right] \ , \tag{9}$$

and $E_g(T_0)$ is the initial field at $T=T_0$. For the full charge compensation, $E_g(T_0)=0$.

As is evident from (8) and (9), the variation of E_g with temperature is determined by the temperature dependence of the pyroelectric coefficient $p(T)$ and effective electrical conductivity $\sigma(T)$ [$\epsilon_g(T)$ and $\epsilon(T)$ are only slowly varying functions of T].

The field increase, according to (8), continues until its value reaches the electric breakdown field E_b. When E_g passes the value E_b, the polarization charge of the crystal quickly decreases because it is compensated by the charge flow produced in the electric breakdown of the ambient gas.

The rate equation for this decrease is given by

$$-\epsilon_0\epsilon\frac{dE_g(t)}{dt}=\sigma^*(E_g,t)E_g(t) \ , \tag{10}$$

where

$$\sigma^*(E_g,t)=\xi\sigma_g(E_g,t) \ , \tag{11}$$

with $\sigma_g(E_g,t)$ standing for the specific conductivity of the ionized gas and ξ $(0<\xi<1)$ being a dimensionless factor characteristic of the breakdown geometry.

The field $E_g(t)$ is given by integrating (10):

$$E_g(t)=E_b\exp\left[-(\epsilon_0\epsilon)^{-1}\int_0^t\sigma^*(E_g,t)dt\right] \ . \tag{12}$$

As t increases, the field $E_g(t)$ keeps decreasing as the breakdown proceeds in time, and the net charge at the active surfaces concomitantly decreases. The mean time which elapses between the start of the breakdown and the voltage drop at a gap distance of the crystal thickness d below the breakdown voltage is dependent on different parameters, especially on the duration of the breakdown time. The latter is determined by the nature of the processes sustaining the breakdown current

[represented by $\sigma^*(E_g,t)$ in (12)]. Paschen[13] found that the breakdown voltage of a spark gap tested under the gas pressure p_g with a gap distance d depends only on the product $p_g d$. Since the breakdown occurs by the ionizing impacts of electrons, the mean free path λ of these electrons is an adequate atomic-physics standard for describing the observation. However, the ionization at the surface, especially in adsorbed layers of the ambient gas, remains insufficient because an effective barrier exists against the acceleration of electrons. Inelastic impacts between electrons and solid-state particles occur, transferring the accumulated kinetic energy of the electrons into excitation energy of the electronic system of the particles. This energy, used for radiation, dissociation, or in impacts of the second kind, will normally be lost for the ionization processes. Consequently, the radiation of the system consists of two components: the emission of the gas particles and the emission characteristic of the crystal (cf. Ref. 7). In addition to the above mechanism of friction, protecting the near-edge gas layers against early breakdown, a decrease in the secondary emission of electrons from an insulating crystal as compared with metallic electrodes must be taken into consideration. In the next section we will see some consequences of these effects by comparison of the Townsend-type discharge in gases with the experimental data from the PEL of an *N*-isopropylcarbazole single crystal.

Our further analysis of the phenomenon is confined to the two temperature intervals

$$T_{b,i-1}+\delta T_{b,i-1}<T<T_{b,i}$$

and

$$T_{b,i}<T<T_{b,i}+\delta T_{b,i} ,$$

where $T_{b,i}$ is the ith temperature value at which the breakdown takes place. While the field at the crystal increases over the first interval, it rapidly drops over the second interval. Thus Eqs. (8) and (12), combined with (7) and (9), give the repeated changes in the field $E_g(T)$:

$$E_g(T)=\begin{cases} W^{-1}(T)\left[E_g(T_{b,i-1}+\delta T_{b,i-1})+\epsilon_0^{-1}\epsilon_g^{-1}\int_{T_{b,i-1}+\delta T_{b,i-1}}^{T} p(T')W(T')dT'\right] & \text{for } T_{b,i-1}+\delta T_{b,i-1}<T<T_{b,i} \quad (13) \\ E_g(T_{b,i})\exp\left[-(\epsilon_0\epsilon\beta)^{-1}\int_{T_{b,i}}^{T}\sigma^*(E_g,T')dT'\right] & \text{for } T_{b,i}<T<T_{b,i}+\delta T_{b,i} , \quad (14) \end{cases}$$

where

$$W(T)=\exp\left[-(\epsilon_0\epsilon\beta)^{-1}\int_{T_{b,i-1}+\delta T_{b,i-1}}^{T}\sigma(T')dT'\right] \quad (15)$$

and $i=1,2,3,\ldots$ are the numbers indicating successive breakdown events with $T_{b,0}=T_0$ and $\delta T_{b,0}=0$. The maximum field $E_g(T_{b,i})$ for the ith breakdown event at temperature $T_{b,i}$ drops rapidly to $E_g(T_{b,i}+\delta T_{b,i})$ with concomitant temperature variation $\delta T_{b,i}$. Equations (13)–(15) are concerned with the electric field strength evolution in the near-edge region of a pyroelectric crystal. But if the optical method is used for observation of the breakdowns, the PEL is measured—the light bursts are recorded successively with temperature variation.

Recalling that

$$E_{b,i}=\int_{T_{b,i-1}}^{T_{b,i}}\frac{dE_g(T)}{dT}dT \quad (16)$$

and assuming for each interval $\Delta T_{i-1,i}=|T_{b,i-1}-T_{b,i}|$ of temperature between consecutive breakdown events (consecutive bursts of light), dE_g/dT is to be characterized by an average value

$$\left\langle\frac{dE_g(T)}{dT}\right\rangle_{\text{av}\,i-1,i}=C_{i-1,i} , \quad (17)$$

we can relate this value to experimentally determined $E_{b,i}$ and $\Delta T_{i-1,i}$ by

$$\left\langle\frac{dE_g(T)}{dT}\right\rangle_{\text{av}\,i-1,i}=E_{b,i}(T)(\Delta T_{i-1,i})^{-1} . \quad (18)$$

If $E_{b,i}(T)=\text{const}$, the temperature dependence $C_{i-1,i}(T)$ [as comes from (13)–(15)] directly determines the temperature repetition rate of the PEL bursts $(\Delta T_{i-1,i})^{-1}$.

III. COMPARISON WITH EXPERIMENT

The purpose of this section is to show how the above phenomenological model of PEL developed for ideal pyroelectric crystals can be applied to treat real crystals exemplified by a single crystal of *N*-isopropylcarbazole ($C_{15}H_{15}N$; the compound will be hereafter referred to as NIPC). The crystal structure of NIPC at room temperature is orthorhombic, space group *Iba*2, with $a=16.808$ Å, $b=17.984$ Å, $c=7.983$ Å, $V=2413.1$ Å^3, and $Z=8$.[14–16] A structural phase transition in NIPC at around 140 K taking place between the C_{2v}^{21} (*Iba*2) high-temperature structure and the C_{2v}^{5} (*Pbc*2_1) low-temperature structure has recently been described[16] and reported earlier in the literature.[4,7,8,17–19] It is suggested to be equivalent to pressure-induced structural transformation at the transition pressure around 0.6 GPa (Refs. 9 and 20) (room temperature). The NIPC crystal is pyroelectric, and thus also piezoelectric, in both phases. The molecular dipole moments are directed along the C—N bonds of the molecules which are

oriented about the direction of the twofold c axis; the spontaneous polarization of the crystal is, therefore, parallel to this axis.

A. Experimental procedures

NIPC was synthesized according to the general method of carbazole alkylation.[21] Crude material was carefully purified by means of repeated crystallization, liquid chromatography, sublimation, and zone refining. The high-quality crystals suitable for PEL measurements were grown from the melt by a Bridgman technique, using a small-diameter glass tube.

Oriented crystals were cleaved with a razor blade into parallepiped-shaped samples (approximately $1\times3\times5$ mm^3) and placed with their (ab) face on a copper cold finger in a cell allowing control of the composition and pressure of the ambient atmosphere over the range $10^{-3}-10^5$ Pa (for a more detailed description and part of the experimental results see Refs. 7 and 8). To verify the basic assumption of the model that the source of the breakdown field is the surface charge generated by temperature change of spontaneous polarization of the crystal, the surface charge measurements were performed simultaneously with detection of the PEL. The setup used for these measurements is shown in Fig. 2. In the measurements of the surface density of polarization charge, the vibrating electrode method was used (see, e.g., Ref. 22). The periodic change (Δl) in the width (l) of the gap between the upper crystal surface and the upper electrode is accompanied by the generation of alternating voltage in the external circuit. The magnitude of that voltage is the measure of the rate of change in the surface density of the charge induced on this electrode and is proportional to the amplitude of electrode vibrations. The voltage amplitude determines the surface density of the charge:

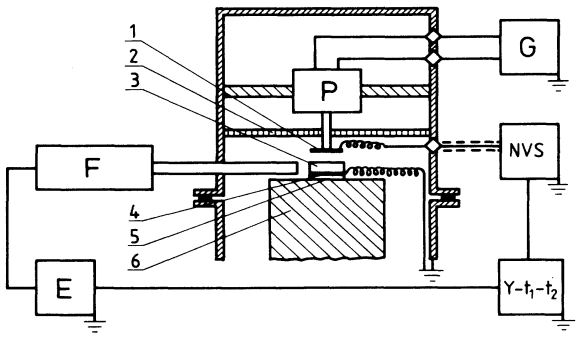

FIG. 2. Schematic of the experimental arrangement for simultaneous measuring of the PEL and surface charge with a pyroelectric crystal. 1, vibrating plate; 2, electrostatic shielding; 3, crystal; 4, metal evaporated electrode; 5, electrically isolating wafer; and 6, cooling or heating copper finger. E, electrometer; F, photomultiplier with a fiber optic leading to the crystal side face; G, ac voltage generator; P, transducer; NVS, selective nanovoltmeter; $Y-t_1-t_2$, two-channel Y-t recorder.

$$\Delta\sigma_S=\frac{Ud}{2\pi f Z_0\,\Delta l\,\epsilon A}\left[\frac{\epsilon l}{d}+1\right]^2. \tag{19}$$

Here U is the measured voltage drop over the impedance Z_0 of the measuring circuit and f is the frequency of the upper electrode vibration.

The measurements of $\Delta\sigma_S$ were carried out at frequency $f=330$ Hz with maximum vibration amplitude $\Delta l=10^{-4}$ m. The luminescence was monitored using a light guide connected to a photomultiplier as shown in Fig. 2. The apparatus allowed the temperature of the crystal to be changed slowly and continuously and the pressure and composition of the ambient atmosphere to be varied.

The measurements of PEL were carried out with different rates (β) of temperature variation, of which the three applied most frequently were 0.0167, 0.083, and 0.2 $K\,s^{-1}$. They could be controlled with about 5% accuracy by an electronic programmable unit over each full experimental cycle. Since the temperature change was realized mainly through the heat exchange at the one plane sample contact with a copper finger, a temperature gradient $\Delta T_d=\beta\rho c\kappa^{-1}d^2$ had to be realized on the crystal. Using, for the density known value $\rho=1.2\times10^3$ $kg\,m^{-3}$ of NIPC and for the heat capacity $c=10^3$ J $kg^{-1}K^{-1}$ and thermal conductivity $\kappa=1$ $W\,m^{-1}K^{-1}$—the values typical of organic solids, we find that the temperature nonuniformity across the crystal thickness $d=10^{-3}$ m increases from $\Delta T_d=0.02$ through 0.1 up to 0.2 K, respectively, to the above three values of β. Similar values of ΔT_d (within a factor of 1.5) have been determined experimentally. Their influence on PEL characteristics is briefly discussed in the next section.

B. Results and discussion

Surface charge measurements indicate that the charge changes synchronously with light emission. The surface density of the charge increases gradually with temperature and time, the increase being observed over a temperature range $\Delta T_{i-1,i}$ correlated to the time elapsed between two successive light pulses (Fig. 3). During this time the electric field $E_g(T)$ is building up to the threshold value of the breakdown field E_b needed to produce the luminescence. The rise time of this charge is followed by its fast decay of duration corresponding to the time of discharge. The oscilloscopic investigations of the light evolution in one burst of PEL from the NIPC crystal surrounded by an argon atmosphere have shown the discharge time to fall in the range 8–25 μs (Fig. 4). This suggests that the breakdown is governed by a relatively slow mechanism, which needs a large number of carrier generations (e.g., some 10^2) to produce a breakdown. Therefore the breakdown has Townsend-type discharge character rather than streamer or Kanalaufbau.[23] It should be noted here that the lower limit of the triplet exciton lifetime in an NIPC crystal is about 1 ms (Ref. 24) and the singlet exciton lifetime does not exceed 20 ns (Ref. 24). Therefore we may conclude that the light pulse duration is not due to the radiative decay of either

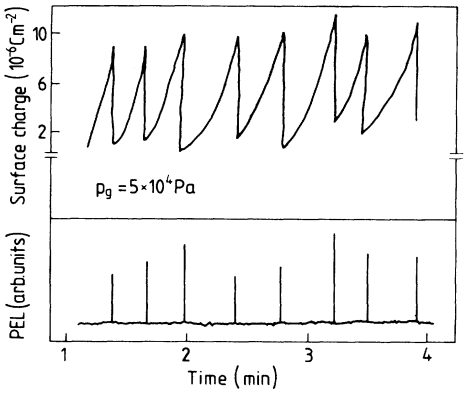

FIG. 3. Bottom: measured intensity of light emitted by a crystal of NIPC when cooled at the rate $\beta=-0.083$ K s^{-1} starting at $\sim$270 K. The pressure of the argon gas surrounding the crystal was $p_g=5\times10^4$ Pa. Top: simultaneous measurement of the surface density of the charge created on the crystal upper surface (see Fig. 2) perpendicular to the pyroelectric axis of the crystal.

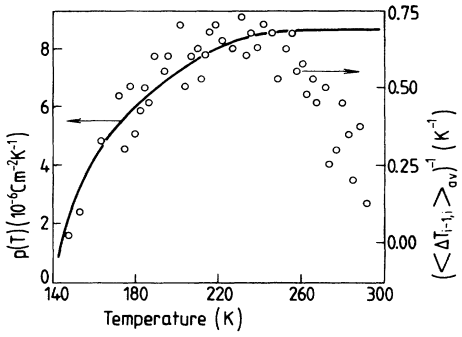

FIG. 5. Circles show the experimental temperature repetition rate $(\langle T_{i-1,i}\rangle_{av})^{-1}$ of the light bursts of the PEL vs temperature. The PEL was induced by cooling with the rate $\beta=-0.2$ K s^{-1} of an NIPC crystal under argon atmosphere at $p_g=8\times10^4$ Pa. This figure also shows data on temperature dependence of the pyroelectric coefficient of the crystal (solid line).

triplet or singlet excitons produced during discharge in the crystal. The results presented in Figs. 3 and 4 provide direct evidence for the correctness and validity of the basic concepts underlying our model for pyroelectric luminescence.

In Fig. 5 the data points represent the reciprocal of the average value of $\Delta T_{i-1,i}$ measured with a crystal of NIPC under argon atmosphere as a function of temperature. The solid line shows the experimental plot of the pyroelectric coefficient. The fluctuation in the production of primary electrons causes the breakdown to be a random process and this leads to a distribution in the values of breakdown field strengths that are measured. Consequently a statistical distribution in the temperature positions of the light pulses of PEL are observed when repeating the cooling or heating run. In a sequence of n runs (usually more than 20) there are $m<n$ repeat positions of a given pulse. Each circle in Fig. 5 corresponds to such a position (T_i) with $m\geq5$. The average temperature distance between $T_{b,i}$ and the temperature of the nearest-neighbor pulse $T_{b,i-1}$ can therefore be defined as

$$\langle\Delta T_{i-1,i}\rangle_{av}=m^{-1}\sum_{j=1}^{m}(\Delta T_{i-1,i})_j\ . \tag{20}$$

Note that for $T=T_{b,i}$ $(i=1,2,3,\ldots)$, $(\Delta T_{i-1,i})_j$ takes on different values with $j=1,2,3,\ldots,m$. The temperature range has been chosen above 140 K in order to avoid possible consequences of the phase transition at $\sim$140 K. Of several different consequences of the phase transition, nonuniform cracking of the sample is the most undesirable, since it would lead to production of triboluminescence[25–28] and additional bursts of light due to local breakdowns at randomly distributed distances shorter than the sample thickness d.

Figure 5 shows the temperature dependence of $(\langle\Delta T_{i-1,i}\rangle_{av})^{-1}$ to follow the temperature change of the pyroelectric coefficient for lower temperatures of the temperature range 140–300 K. They are different, however, in the higher-temperature region where the temperature repetition rate of PEL burst shows apparent increase with cooling or decrease with heating of the crystal. This result is a consequence of the fact that $\langle dE_g(T)/dT\rangle_{av\,i-1,i}$ [see (18)] is a functional of both temperature dependence of $p(T)$ and $\sigma(T)$. Whereas $p(T)$ (as comes from the experiment) becomes constant above $\sim$250 K, the effective conductivity of the system is expected to be still varying. In order to get an estimate of the effect of varying $\sigma(T)$ we have measured the temperature dependence of the effective conductivity in the NIPC crystal with electrodes placed on the sample in a way which allowed the summarized measurement of the bulk and surface conductivities (see the inset in Fig. 6; the electrode system consisted of two parallel evaporated silver layers extended slightly with a silver paste to the side faces of the crystal). The measure of σ is the quantity $\sigma'=d/R$, where R is the effective resistance of the sample. In Fig. 6 the temperature dependence of σ' is shown to follow an Arrhenius law,

$$\sigma'(T)=\sigma'_0\exp(-\Delta E/kT)\ , \tag{21}$$

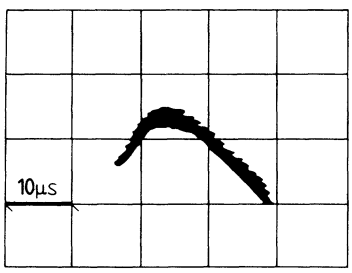

FIG. 4. Typical oscillogram of the PEL light burst observed with an NIPC crystal under argon atmosphere.

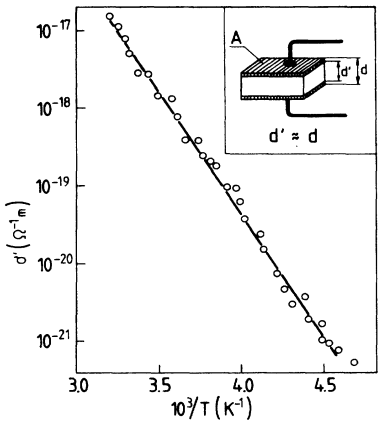

FIG. 6. Temperature dependence of σ' [Eq. (21)] expressing the temperature variation of the effective conductivity of an NIPC crystal sample. The NIPC crystal with arrangement of electrodes is shown in the inset ($d=1.2\times10^{-3}$ m, $A=5\times10^{-6}$ m^2, and the voltage applied is $U=10^3$ V).

with the activation energy $\Delta E\cong0.6$ eV and preexponential factor $\sigma_0'\cong\sigma'(T_0)\exp(\Delta E/kT_0)$ in which $\sigma'(T_0)=5\times10^{-18}\ \Omega^{-1}$ m at room temperature ($T_0=300$ K).

We can now calculate the near-crystal-edge electric field E_g by substituting Eq. (21) into Eq. (15) and then making use of Eq. (13). [Note that $\sigma(T)=\sigma'(T)/A$.] The results of such a calculation are represented by curves in Fig. 7, where E_g as a function of temperature

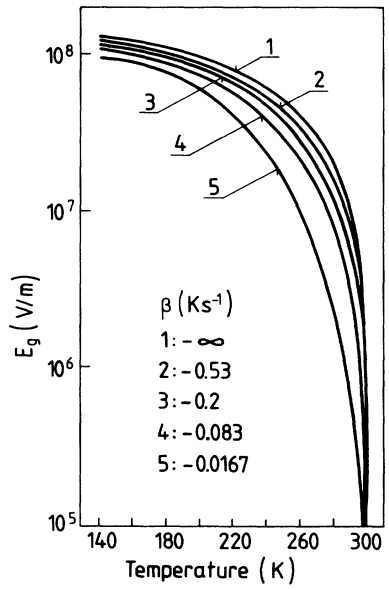

FIG. 7. Calculated temperature dependence of the near-crystal-edge field (E_g) as a function of the rate of the crystal cooling (β). The calculation is based on Eq. (13) and experimental plots of $p(T)$ and $\sigma(T)$ with $\epsilon(T)\cong$const$=3.7$ (Ref. 17).

for its five different changing rates is displayed. It is seen that in all the cases the field increases rapidly at the first stage of cooling and then tends to saturate at the value $\sim10^8$ V/m, which is about one order of magnitude lower than the polarization field (1) as estimated with the molecular dipole moment of NIPC; $\mu_i\approx10^{-29}$ C m (cf. Ref. 9). The temperature evolution of $E_g(T)$ can, however, be disrupted below this limiting field due to a breakdown event at the crystal edge, as expressed by Eq. (14). The rate of temperature change of E_g is a measure of the repetition rate of PEL burst $(\Delta T_{i-1,i})^{-1}$ (18). The expression for this rate in form (17) has been evaluated on the basis of Eq. (13) and on the experimental data of $p(T)$ and $\sigma(T)$ for comparison to experimental dependence of the repetition rate $(\langle\Delta T_{i-1,i}\rangle_{\rm av})^{-1}$ on temperature. The comparison is shown in Fig. 8. From this comparison we conclude that the model presented in Sec. II provides a good description for the repetition rate of light bursts characteristic of PEL phenomenon. It indicates that the high-temperature drop in the repetition rate is due to increasing conductivity in the bulk and mainly at the surface of the crystal. This observation is consistent with the physical picture of PEL. Increasing conductivity [with $p(T)=$const] causes a dropoff in the temperature-induced increment of the net surface charge; hence more time is required for the field to reach its breakdown value and the repetition rate of the light bursts decreases. Figure 8 shows that an increase in the cooling rate leads to a stronger scatter of experimental values of the repetition rate (open circles). It can be associated with a contribution of the so-called tertiary pyroelectric effect (see, e.g., Ref. 29). The temperature gradient on the sample produces an additional polarization which modifies the value and temperature dependence of the pyroelectric coefficient. The effect of changing $p(T)$, negligible as measured at low β rates, becomes slightly

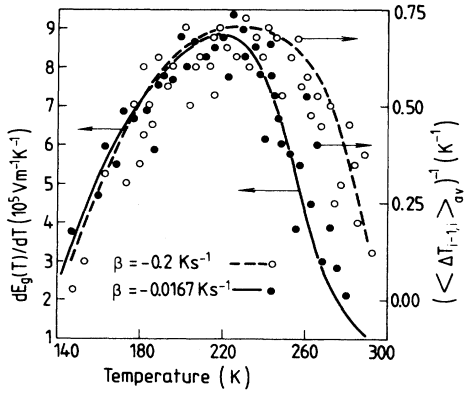

FIG. 8. Temperature repetition rate of PEL bursts as a function of temperature. Open and solid circles show the experimental repetition rate (the right-hand scale) for two different values of the cooling rate. Solid and dashed lines are the corresponding theoretical plots of the temperature derivative of $E_g(T)$ which to a constant factor $E_{b,i}$ is a measure of $(\Delta T_{i-1,i})^{-1}$ [Eq. (18)] (the left-hand scale). The theoretical curves are based on Eq. (13) in the text.

noticeable at $\beta=0.2\ \mathrm{K}^{-1}$. These observations are compatible with the experimental conditions causing the temperature nonuniformity across the crystal to increase with increasing β (see Sec. III A). At sufficiently high β rates and thick samples the tertiary pyroelectric effect should be explicitly introduced into the model. However, under the experimental conditions of the present work it can be considered as a perturbation of secondary importance, slightly affecting the intensity of individual PEL bursts and increasing the scatter of experimental points for the repetition rate. The influence of a possible nonuniformity of the temperature distribution in gas surrounding the sample can be disregarded, since the breakdown events take place on crystal surfaces, where the temperature field is determined by the crystal itself.

In comparing the experimental results on NIPC crystals with those of other researchers,[1-3,5] one can see the difference concerning the temperature dependence of the repetition rate; whereas in the case of NIPC it shows a maximum at about 230 K, the repeating pattern of light bursts in other works is suggested to be almost periodic over the entire temperature range. This would indicate that the other crystals are characterized by either weak temperature-dependent functions of pyroelectric coefficient and electrical conductivity, or by their similar temperature changing in the same direction. However, it should be recognized that the detailed analysis of the temperature distribution of PEL bursts has not been made to date; hence neither of these suggestions have been sufficiently justified and they need further revision.

Additional evidence for the validity of our model may be drawn from the analysis of ambient-gas-pressure dependence of PEL. The temperature separation between two subsequent bursts of light was measured for various ambient gases at pressures above 10^2 Pa, over the temperature range 190–275 K.[7] For all gases employed (He, Ne, Ar, N_2, O_2, and SF_6), $\Delta T_{i-1,i}$ is approximately a power (s) function of the pressure (p_g) being generally larger for gases characterized by higher values of the electrical breakdown field:

$$\langle \Delta T_{i-1,i} \rangle_{\mathrm{av}\,N}(p_g) \sim p_g^s \quad \text{with } 0.23 \lesssim s \lesssim 0.48 \ . \tag{22}$$

In this relation the average is taken over the entire temperature range for many runs as

$$\langle \Delta T_{i-1,i} \rangle_{\mathrm{av}\,N} = N^{-1} \sum_{i=1}^{N} \Delta T_{i-1,i} \ , \tag{23}$$

where N is the total number of light bursts recorded in a sequence of temperature runs [note the difference with respect to the average given by (20)].

These features of $\langle \Delta T_{i-1,i} \rangle_{\mathrm{av}\,N}$ strongly suggest that the breakdown is in fact a precondition of PEL. The breakdown field created by a pyroelectric sample can be directly related to changes in spontaneous polarization by

$$E_b(p_g) = (\epsilon_0 \epsilon_g)^{-1} \langle p(T) \rangle_{\mathrm{av}} \langle \Delta T_{i-1,i} \rangle_{\mathrm{av}\,N} \tag{24}$$

[see definition of $p(T)$ (4)]. For comparison of $E_g(p_g)$ with the breakdown field of a gas between plane-parallel metal electrodes, the temperature average of $p(T)$ is introduced in Eq. (24). The comparison is shown in Fig. 9 in the form of a conventional Paschen's dependence: $E_b = f(p_g d)$, p_g being the pressure of argon surrounding a crystal of NIPC, and d denoting the interelectrode distance. In the calculation of $E_g(p_g)$ d was assumed to be equal to the crystal thickness. By its pressure increase, the breakdown field strength follows the Paschen's relation for the breakdown voltage (see, e.g., Ref. 30):

$$U_g = \frac{B_0(p_g d)}{\ln(p_g d) + \ln[A_0 / \ln(1+\gamma^{-1})]} \ , \tag{25}$$

where A_0 and B_0 are constants characteristic of the gas and γ is the second Townsend coefficient involving photoemission of electrons from the cathode.

However, the values of E_b calculated from (24) are a factor of ~ 2 larger than those from the data in the literature on breakdown in argon. The possibility of the influence of electrode dependent γ has been considered and the results with $\gamma = 10^{-3}\gamma_{\mathrm{metal}}$ obtained from (25). These results show the Paschen's plot shifting up about 15%, which does not remove the discrepancy. Suspecting that it arises from the temperature averaging of $p(T)$ and neglecting $\sigma(T)$, we calculated E_b from the model according to Eqs. (13)–(15) for $E(T_{b,i} + \delta T_{b,i}) = 0.2E(T_{b,i})$, the latter taken from the temperature-averaged $\Delta\sigma_S(T)$ (see Fig. 3) and relation (3). The result, plotted in Fig. 9, shows no difference within the error of the data. This means that in practice the pressure dependence of $\Delta T_{i-1,i}$ and thus E_b is identical within the entire temperature range, reflecting the breakdown to be a property of the gas. Also shown in Fig. 9 is the breakdown field calculated from Eq. (3) based on the experimental (average) values of $\Delta\sigma_S$ (see Fig. 3). The lower values of E_b in this case are most probably due to

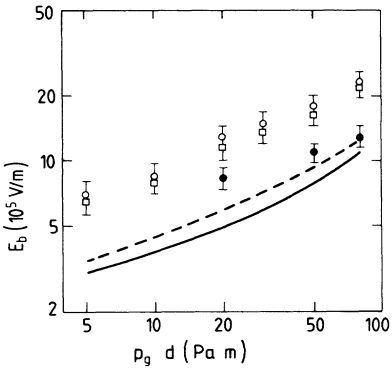

FIG. 9. Dependence of the breakdown field in argon on the product $p_g d$. Circles and squares denote the breakdown field created by a 1-mm-thick NIPC crystal; ○, obtained from relation (24), $\epsilon_g = 1$; □, based on the model calculations from Eqs. (13)–(15) (see text); ●, determined from Eq. (3) on the basis of the experimental data for σ_S from Fig. 3; solid line, breakdown field between plane-parallel metal electrodes (taken from Ref. 23); dashed line, the Paschen's curve according to Eq. (25) with $\gamma = 10^{-3}\gamma_{\mathrm{metal}}$.

inhomogeneous distribution of the surface charge. The side surface conductivity causes the lower near-edge values of $\Delta\sigma_S$ to be closer to those responsible for the actual breakdown field when E_b determined from PEL is based on the values of $p(T)$ measured in the central part of the crystal [note that the dimensions of the vibrating electrode in the arrangement measuring $\Delta\sigma_S$ (Fig. 2) are comparable with the crystal dimensions; thus measured $\Delta\sigma_S$ is an average over the charged surface]. While for the largest values of $p_g d$ agreement between such determined E_b and gas data with a spark gap between metal electrodes is satisfactory, disagreement appears for smaller products $p_g d$ (Fig. 9). The difference is probably related to decreasing surface conductivity.

Finally, it seems that, in addition to the surface character of the breakdown, the inhomogeneous surface charge distribution causes the discrepancy between our values of E_b and those from the Paschen's dependence described in the literature. Due to the near-edge decrease of $\Delta\sigma_S$ it might also be expected that the discharge path is longer than the crystal thickness d. This would lead to a lowering of E_b and its better agreement with the data in the literature on the gas discharge. Since, however, the conditions at the surface of the crystal are difficult to determine anyway, it is not possible to ascribe more physical meaning to E_b at present except to treat it as an adjustable parameter. Equations (13)–(15) are used to analyze $\langle \Delta T_{i-1,i} \rangle_{\mathrm{av}\,N}$ as a function of pressure, employing the Paschen's dependence described in the literature for different gases as a basis for $E_b(p_g)$. Figure 10 summarizes the results for four different gases. The agreement between theoretical predictions of the pressure dependence of the average repetition interval of the PEL bursts and experimental data is very good and increases our confidence in the validity of the assumptions made in the derivation of the theoretical model. The only deviation from the theoretical predictions is the difference in the absolute values of $\langle \Delta T_{i-1,i} \rangle_{\mathrm{av}\,N}$ which comes from the above-discussed discrepancy in E_b.

In summary, we have shown how temperature and pressure dependencies can arise in pyroelectric luminescence light bursts and have obtained qualitative agreement with experiment. We evaluate the temperature repetition rate of the bursts from the balance equation of the charge on the pyroelectric faces, that is, from the equations describing the dynamics of this surface charge under different conditions of temperature variation and of characteristics of the gas surrounding pyroelectric crystals. We show how the effective conductivity of the crystal-gas system can be incorporated into the theoretical model and then verified in experiment. The gratifying feature about the basic agreement between the model and experiment is that the premises underlying the theory are obviously sufficiently adequate to enable the pyroelectric luminescence to be treated.

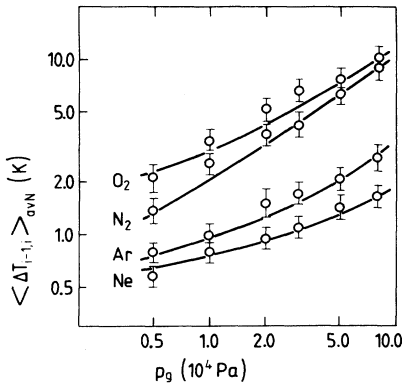

FIG. 10. Comparison of the theoretical (solid lines) and experimental (circles) data of the average temperature separation between two subsequent bursts of light as a function of the pressure of various ambient gases for a crystal of NIPC. The temperature average is taken according to Eq. (23). Theoretical data are calculated from Eq. (18) with $E_{b,i}$ taken from suitable Paschen's plots from the literature (Ref. 30). The excellent fit between the experimental data and the theory over the entire pressure range has been obtained by multiplying the calculated data by the following numerical factors: 2.76 for O_2, 1.87 for N_2, 2.14 for Ar, and 2.20 for Ne.

ACKNOWLEDGMENT

The work was supported in part by the Polish Academy of Sciences under Program No. CPBP 01.12.

[1] J. S. Patel and D. M. Hanson, Nature (London) **293**, 445 (1981).

[2] J. S. Patel and D. M. Hanson, Ferroelectrics **38**, 923 (1981).

[3] D. M. Hanson, J. S. Patel, I. C. Winkler, and A. Morrobel-Sosa, in *Spectroscopy and Excitation Dynamics of Condensed Molecular Systems,* Vol. 4 of *Modern Problems in Condensed Matter Sciences,* edited by V. M. Agranovich and R. M. Hochstrasser (North-Holland, Amsterdam, 1983), p. 659.

[4] Z. Dreger, J. Kalinowski, R. Nowak, and J. Sworakowski, Mater. Sci. **10**, 67 (1984).

[5] D. M. Hanson, J. S. Patel, and M. C. Nelson, Mater. Sci. **10**, 459 (1984).

[6] K. S. V. Nambi, Phys. Status Solidi A **82**, K71 (1984).

[7] Z. Dreger, J. Kalinowski, R. Nowak, and J. Sworakowski, Chem. Phys. Lett. **116**, 192 (1985).

[8] Z. Dreger, Ph.D. thesis, Technical University of Gdańsk, 1986 (unpublished).

[9] J. Kalinowski, J. Godlewski, Z. Dreger, and P. Mondalski, Chem. Phys. Lett. **128**, 480 (1986).

[10] G. Schmidt and J. Peterson, Z. Naturforsch. Teil A **24**, 1559 (1969).

[11] G. Schmidt, J. Peterson, and H. E. Muser, Suppl. J. Phys. Soc. Jpn. **28**, 147 (1970).

[12] S. B. Lang, *Sourcebook of Pyroelectricity* (Gordon and Breach, New York, 1974), Chap. 1.

[13] F. Paschen, Ann. Phys. (Leipzig) **37**, 69 (1889).

[14] P. Cherin and M. Burack, J. Phys. Chem. **70**, 1470 (1966).

[15] O. Saravari, N. Kitamura, S. Tazuke, A. Takenaka, and Y. Sasada, Acta Crystallogr. C **40**, 1617 (1984).

[16] F. Baert, A. Mierzejewski, B. Kuchta, and R. Nowak, Acta Crystallogr. B **42**, 187 (1986).

[17] R. Nowak and R. Poprawski, Ferroelectrics Lett. **1**, 175

(1984).
[18]R. Nowak, J. Sworakowski, R. Kowal, J. Dziedzic, and R. Poprawski, Ferroelectrics **65**, 79 (1985).
[19]M. Bertault, A. Collet, and R. Nowak, Solid State Commun. **58**, 613 (1986).
[20]J. Kalinowski, J. Godlewski, Z. Dreger, and P. Mondalski, in Proceedings of the International Symposium on Molecular Luminescence and Photophysics, Toruń, Poland, 1986 (unpublished).
[21]T. Stevens and S. H. Tucker, J. Chem. Soc. **123**, 2140 (1923).
[22]W. A. Zisman, Rev. Sci. Instrum. **3**, 366 (1932); L. A. Freedman and L. A. Rosenthal, *ibid.* **21**, 896 (1950).
[23]A. Engel, *Ionized Gases* (Clarendon, Oxford, 1955), Chap. 7, Sec. 5; H. Raether, *Electron Avalanches and Breakdown in Gases* (Butterworths, London, 1964), Chap. 5.
[24]Z. Dreger, J. Kalinowski, B. Kozankiewicz, and J. Prochorow (unpublished).
[25]A. J. Walton, Adv. Phys. **26**, 887 (1977).
[26]B. P. Chandra and J. I. Zink, J. Chem. Phys. **73**, 5933 (1980); Phys. Rev. B **21**, 816 (1980).
[27]R. Nowak, A. Krajewska, and M. Samoć, Chem. Phys. Lett. **94**, 270 (1983).
[28]N. Kitamura, O. Saravari, H. B. Kim, and S. Tazuke, Chem. Phys. Lett. **125**, 354 (1986).
[29]W. L. Gurevitch, Fiz. Tverd. Tela (Leningrad) **23**, 2357 (1981) [Sov. Phys.—Solid State **23**, 1377 (1981)].
[30]J. M. Meek and J. D. Craggs, *Electrical Breakdown of Gases* (Clarendon, Oxford, 1953), Chap. 2.